

## Fluorescence

## Coumarin-3-Aldehyde as a Scaffold for the Design of Tunable PET-Modulated Fluorescent Sensors for Neurotransmitters

Kenneth S. Hettie and Timothy E. Glass\*<sup>[a]</sup>

**Abstract:** NeuroSensor 521 (NS521) is a fluorescent sensor for primary-amine neurotransmitters based on a platform that consists of an aryl moiety appended to position C4 of the coumarin-3-aldehyde scaffold. We demonstrate that sensors based on this platform behave as a directly linked donor–acceptor system that operates through an intramolecular acceptor-excited photoinduced electron transfer (a-PET) mechanism. To evaluate the PET process, a series of benzene- and thiophene-substituted derivatives were prepared and the photophysical properties, binding affinities, and fluorescence responses toward glutamate, norepinephrine, and dopamine were determined. The calculated energy

of the highest occupied molecular orbital ( $E_{\text{HOMO}}$ ) of the pendant aryl substituents, along with oxidation and reduction potential values derived from the calculated molecular orbital energy values of the platform components, allowed for calculation of the fluorescence properties of the benzene sensor series. Interestingly, the thiophene derivatives did not fit the typical PET model, highlighting the limitations of the method. A new sensor, NeuroSensor 539, displayed enhanced photophysical properties aptly suited for biological imaging. NeuroSensor 539 was validated by selectively labeling and imaging norepinephrine in secretory vesicles of live chromaffin cells.

## Introduction

Fluorescence imaging, in its many forms, has become the premier method for unraveling complex biological problems.<sup>[1]</sup> A variety of probes are available for fluorescent labeling of macromolecules; however, small-molecule imaging often requires the use of fluorescent chemical sensors.<sup>[2]</sup> An important goal in this field remains the ability to rationally design fluorescent probes and sensors. Recently, Nagano has shown that several fluorophores act as directly linked donor–acceptor systems (Figure 1) in which a pendant aryl moiety that is orthogonal to and not conjugated with the fluorophore can modulate the fluorescence output by intramolecular photoinduced electron

transfer (PET).<sup>[3]</sup> This PET quenching can occur in either a donor- or acceptor-excited mechanism, and balancing the electronics of the system is key to obtaining the desired fluorescence properties.

To describe these systems in a quantitative fashion, the rate of electron transfer ( $k_{\text{ET}}$ ) between the excited state fluorophore (scaffold) and the pendant aryl moiety was determined from the free energy change for electron transfer ( $\Delta G_{\text{ET}}$ ) using the Marcus equation. In turn,  $\Delta G_{\text{ET}}$  values were determined from the Rehm–Weller equation using experimentally measured oxidation and reduction potentials of the platform components.<sup>[3]</sup> The data could then be used to calculate the fluorescence quantum yields ( $\Phi_{\text{f}}$ ) of the derivatives. Most importantly,

Nagano demonstrated a direct relationship between the experimentally determined quantum yield and the calculated energy of the highest occupied molecular orbital ( $E_{\text{HOMO}}$ ) of the corresponding pendant aryl moiety. This relationship greatly facilitates the a priori determination of fluorescence output. However, to be truly quantitative, it was necessary to have the experimentally determined oxidation

potential of the unsubstituted scaffolds (fluorophores). Thus, only the xanthene and BODIPY scaffolds have undergone quantitative evaluation. However, the method has been used for qualitative assessment of fluorescence properties based on platforms consisting of modified scaffolds.<sup>[4]</sup>

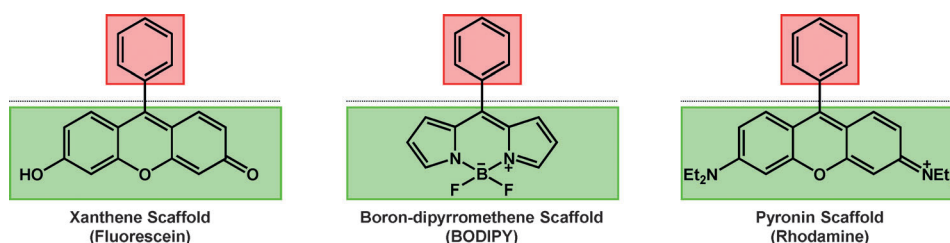


**Figure 1.** Platforms that consist of a directly linked donor–acceptor system which exhibit intramolecular PET between an orthogonal pendant aryl moiety and an excited state fluorophore (scaffold).

[a] K. S. Hettie, Prof. T. E. Glass  
Department of Chemistry, University of Missouri  
Columbia, MO 65211 (USA)  
E-mail: glassst@missouri.edu

Supporting information for this article is available on the WWW under <http://dx.doi.org/10.1002/chem.201403128>.

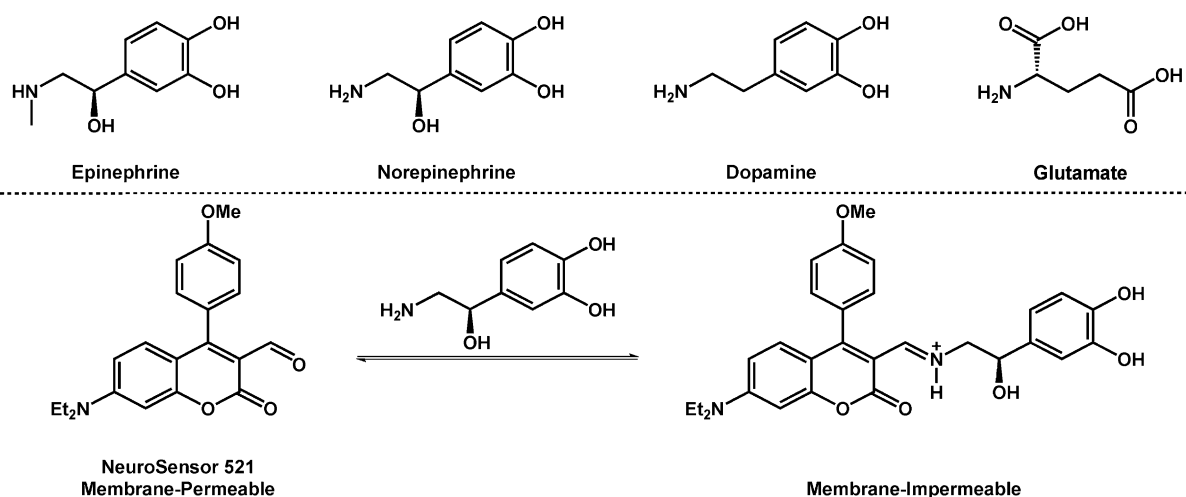


**Figure 2.** Structures of select neurotransmitters. Structure of NS521 and formation of the iminium ion upon interaction with norepinephrine.

Some time ago, we developed a ditopic fluorescent molecular sensor that exhibited good selectivity toward catecholamines.<sup>[5]</sup> The sensor operated in a turn-off mode due to quenching of the fluorophore by the catechol group. More recently, we developed NeuroSensor 521 (NS521) as a turn-on fluorescent sensor for the catecholamines norepinephrine and dopamine (Figure 2).<sup>[6]</sup>

NS521 derives from the coumarin-3-aldehyde scaffold, wherein the aldehyde group associates with the analyte primary amine group by reversible iminium ion formation.<sup>[7]</sup> The coumarin aldehyde fluoresces from an internal charge transfer (ICT) state.

Formation of the iminium ion stabilizes the ICT state and shifts the wavelength of absorbance from 448 to 488 nm, allowing the bound and unbound forms of the sensor to be independently monitored by appropriate selection of the excitation wavelength. In principle, the aldehyde group of NS521 can interact with any intracellular free primary amine. However, the low binding affinities of NS521 toward free primary amines ( $\approx 10 \text{ M}^{-1}$ ) coupled with the low concentration of intracellular free primary amines (5 mM) translates into extremely weak associations and thus, NS521 remains largely unassociated upon exposure to typical cells. However, specialized neurons sequester and package individual primary-amine neurotransmitters (e.g., glutamate, norepinephrine, dopamine, and serotonin) in secretory vesicles at extremely high concentrations (300 mM–1 M) within an acidic environment ( $\approx \text{pH } 5$ ).<sup>[8]</sup> We envisaged that the neutral NS521 would diffuse into the secretory vesicles of such specialized cells and only bind with the primary amine neurotransmitter due to the extremely high concentration of the bioanalyte. In turn, the resultant imine form of NS521 would become protonated to form a charged complex due to the acidic environment within secretory vesicles and become membrane impermeable (Figure 2). As a result, the sensor would accumulate inside the secretory vesicles and allow for clear visualization of the neurotransmitter with low background. NS521 was initially validated in chromaffin cells and demonstrated selective detection of norepinephrine, allowing

discrimination between norepinephrine- and epinephrine-enriched cell populations.<sup>[6]</sup> While NS521 was validated with norepinephrine, it also responds well to dopamine. Theoretically, NS521 could bind to any cellular primary amine; however, specialized neurons (e.g., dopaminergic, glutamatergic, and serotonergic) specifically package one neurotransmitter at high concentrations (hundreds of millimolar) and can be isolated from their respective locales in the brain. Specificity is gained from the combined effect of a singly concentrated neurotransmitter and the modest binding affinities for this class of molecular sensor in order to afford visualization of only the desired neurotransmitter.

Since the fluorescent imaging of neurons, neurotransmitters, and events surrounding synaptic firing is an increasingly active area of research, the potential applications of such sensors are profuse. Fluorescent sensors would enhance research in neuroscience by providing both the imaging of primary-amine neurotransmitters (especially for neurotransmitters such as dopamine that tend to quench fluorescence) and the continuous monitoring of primary-amine neurotransmitter trafficking. Therefore, we sought to establish a model by which sensors could be rationally designed for the purposes of neuroimaging. Because the NS521 platform consists of a fluorophore (scaffold) with a pendant orthogonal aromatic group, we designed various NS521 analogues and applied Nagano's method to this unique sensor system to evaluate the photophysical interaction between the platform components.

Herein, we report a series of benzene- and thiophene-substituted sensors based on the coumarin-3-aldehyde scaffold. The photophysical properties, binding affinities, and fluorescence responses toward glutamate, norepinephrine, and dopamine were experimentally determined. DFT calculations provided the energy of the highest occupied molecular orbital ( $E_{\text{HOMO}}$ ) values of the pendant aryl substituents (calculated at the B3LYP/6-31G(d) level of theory), which were fine-tuned through the introduction of various electron-withdrawing and -donating groups. In conjunction with the Marcus theory of electron transfer, oxidation and reduction potential values strictly de-

rived from the calculated molecular orbital energy values of the fluorophore allowed for calculation of the fluorescence properties of the sensors. Good agreement between the calculated and experimentally determined fluorescence properties was found only in the case of the benzene-substituted sensors.

## Results

### Design and synthesis of NS521 derivatives

To systematically investigate the directly linked intramolecular PET in this system, a series of benzene- and thiophene-substituted derivatives based on the coumarin-3-aldehyde scaffold were prepared (Figure 3 A). Substituents on the C4 aryl groups were chosen to cover a wide range of calculated  $E_{\text{HOMO}}$  values (Figure 3 B). The primary difference between the two classes of aryl moieties is the dihedral angle of the pendant aryl moiety with respect to the plane of the coumarin aldehyde scaffold. The thiophene class was determined to maintain a smaller dihedral angle ( $72.1^\circ$ ) compared to the benzene class ( $82.3^\circ$ ) based on geometry-optimized structures. For the purpose of discussion, it is noted that the only *ortho*-substituted derivative (**1 h**) was determined to have a larger dihedral angle ( $89.3^\circ$ ).

The sensors were prepared as shown in Scheme 1. The synthesis of the benzene-based sensors (**1 a–l**) and the benzothio-

phene sensor (**2 e**) was achieved through a single Suzuki coupling reaction with compound **3** to provide the final products. The thiophene-based sensors (**2 a–d**) were synthesized in two steps from compound **5** through tosylation and coupling followed by formylation under Vilsmeier conditions.

### Spectroscopic properties

The sensors were titrated with glutamate as a representative amine and the absorption and fluorescence spectra recorded in buffer at pH 5 to mimic the acidic interior of the secretory vesicle. Representative spectral changes for sensors **1 b** and **2 b** upon binding with analyte are shown in Figure 4. As observed with other sensors in this series, interaction with a primary amine produces a redshift in absorption. For the series **1** sensors, the absorption of the bound species shifted from approximately 448 to 488 nm. Similarly, the emission maxima of the series **1** sensors were redshifted to approximately 520 nm upon binding, giving these sensors spectroscopic properties that conveniently match that of fluorescein. For the series **2** sensors, the absorbance shifts from approximately 467 to 502 nm upon interaction with glutamate and the emission shifts from approximately 522 to 540 nm, which is 20 nm longer in wavelength than the absorbance values for the series **1** sensors. The fluorescence quantum yields ( $\Phi_{\text{fl}}$ ) of the

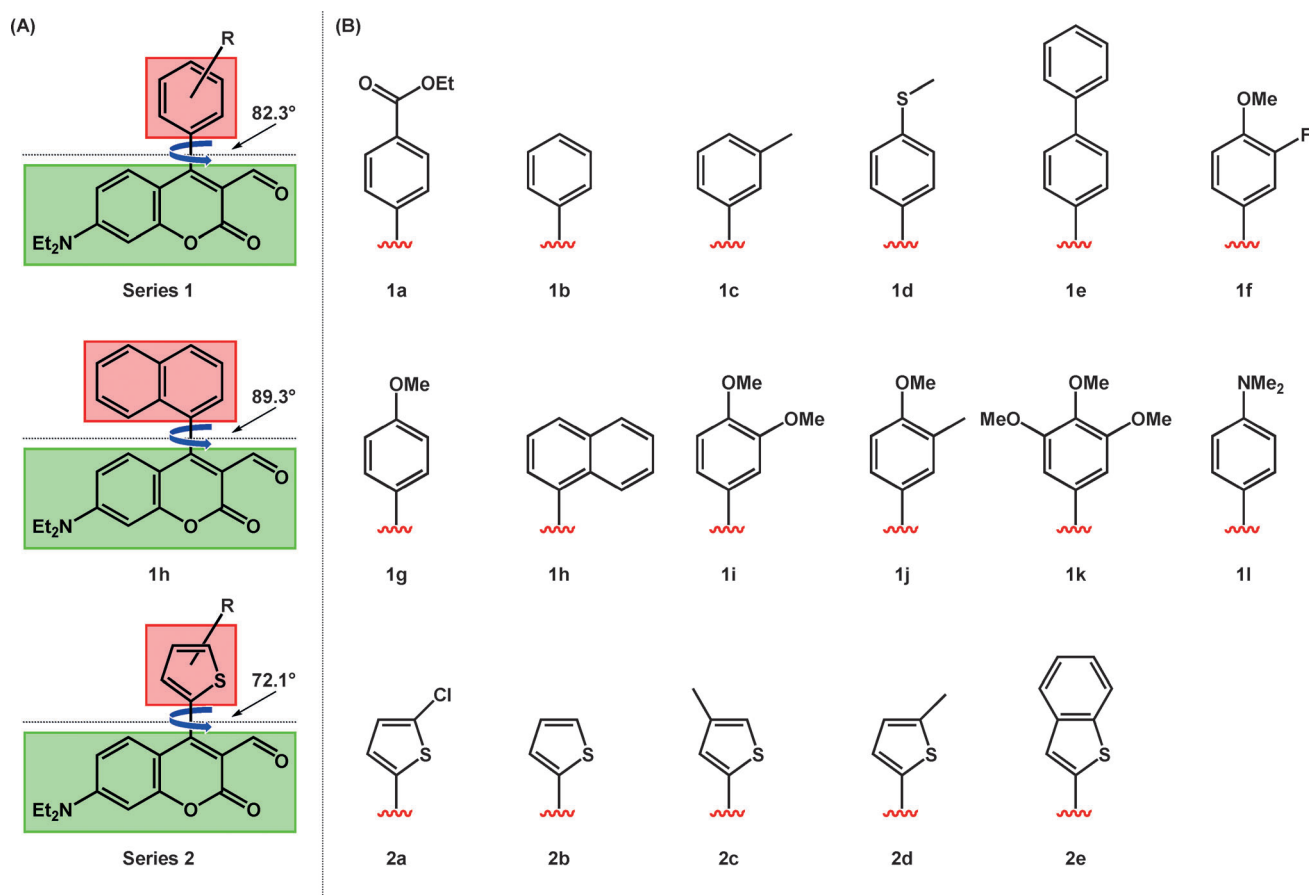
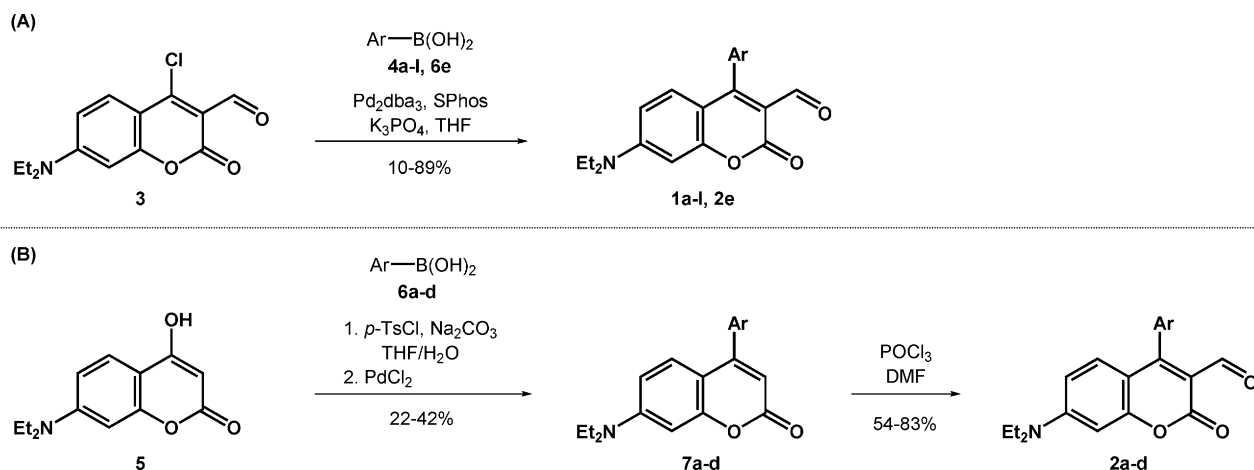


**Figure 3.** A) The sensor platform consists of a pendant aryl moiety (red) directly linked to position C4 of the coumarin-3-aldehyde scaffold (green). B) Structures of derivatives used in this study: benzene-substituted series (**1 a–l**) and thiophene-substituted series (**2 a–e**).



Scheme 1. Synthesis of A) benzene- and B) thiophene-substituted sensors based on the coumarin-3-aldehyde scaffold.

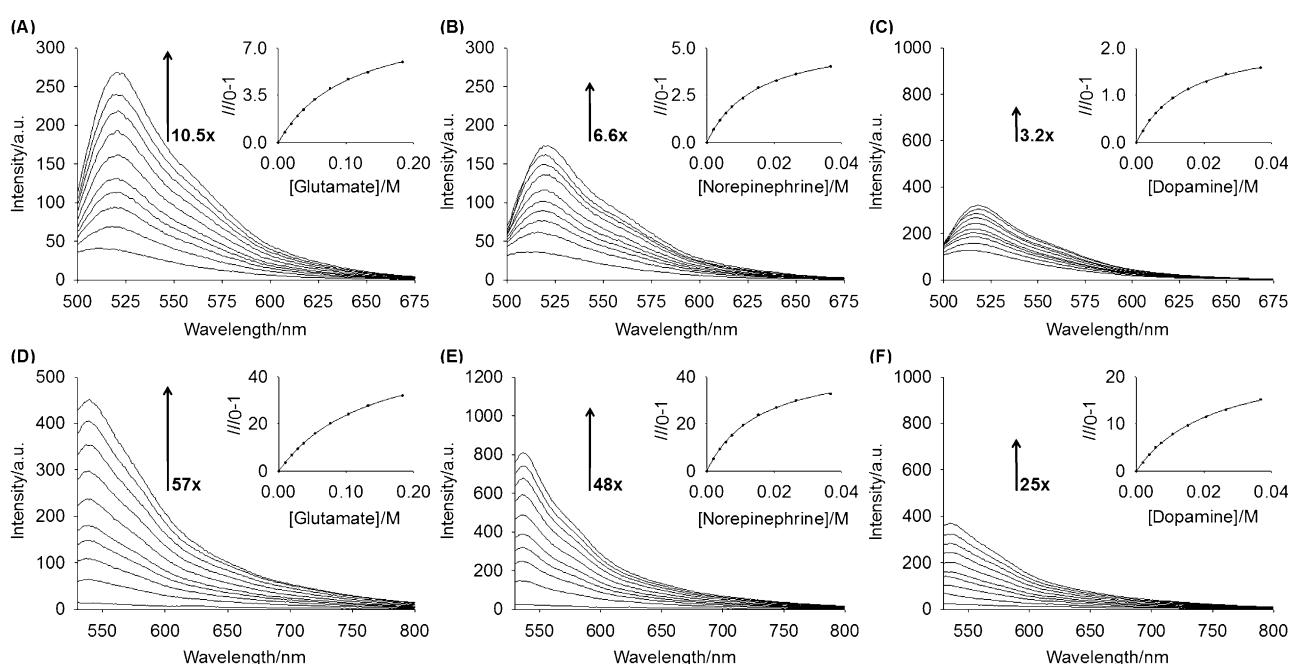


Figure 4. Fluorescence titration of sensor **1b** (10  $\mu\text{M}$ ) with 0, 20, 40, 60, 80, 120, 180, 260, 360, and 580  $\mu\text{L}$  of A) 500 mM glutamate, B) 100 mM norepinephrine, and C) 100 mM dopamine. Fluorescence titration of sensor **2b** (10  $\mu\text{M}$ ) with 0, 20, 40, 60, 80, 120, 260, 360, and 580  $\mu\text{L}$  of D) 500 mM glutamate, E) 100 mM norepinephrine, and F) 100 mM dopamine. Fluorescence titrations were performed in buffer (25 mM HEPES, 50 mM  $\text{Na}_2\text{S}_2\text{O}_3$ , pH 5.0, 37  $^\circ\text{C}$ ) with excitation at 488 and 515 nm for sensors **1b** and **2b**, respectively. Insets are fits to a one-site binding isotherm. Fluorescence enhancements were calculated from  $I_{\text{sat}}/I_0$ , where  $I_{\text{sat}}$  is the maximum fluorescence at saturation taken from the theoretical fit to the binding isotherm and  $I_0$  is the initial fluorescence of the sensor.

unbound and bound sensors were measured in buffer at pH 5.0 and tabulated in Table 1. Full detailed photophysical properties including calculated  $E_{\text{HOMO}}$  and  $E_{\text{LUMO}}$  values are tabulated in Tables S1 and S2 in the Supporting Information.

### Binding affinities

The association constants ( $K_a$ ) of each sensor toward glutamate, norepinephrine and dopamine are listed in Tables 2 and 3 for series **1** and **2**, respectively. The interaction between coumarin aldehydes and primary amines is a covalent reaction and, in principle, would be best represented as an equilibrium

constant ( $K_{\text{eq}}$ ). However, because most supramolecular interactions are measured in terms of an association constant, we have adopted that convention here for the sake of comparison and ease of use. Tables 2 and 3 also list maximum fluorescent enhancements ( $I_{\text{sat}}/I_0$ ), which are the fluorescence intensities at saturation (as determined by the fit to a one-site binding isotherm) relative to the fluorescence intensities of the unbound sensors. These data give the maximum possible fluorescence response and are useful in comparing the spectroscopic properties of the fully bound sensor to the unbound state as well as to other sensors.

**Table 1.** Quantum yields for series 1 and 2 sensors.

Pendant aryl moiety	Quantum yield <sup>[a]</sup>	
	Unbound <sup>[b]</sup>	Bound <sup>[c,d]</sup>
4-carbethoxy ( <b>1 a</b> ) <sup>[e]</sup>	0.0054	0.0100
phenyl ( <b>1 b</b> )	0.0072	0.0128
3-methyl ( <b>1 c</b> )	0.0069	0.0102
4-methylthio ( <b>1 d</b> )	0.0067	0.0101
4-biphenyl ( <b>1 e</b> ) <sup>[f]</sup>	0.0085	0.0150
3-fluoro-4-methoxy ( <b>1 f</b> )	0.0063	0.0097
(NS521) 4-methoxy ( <b>1 g</b> )	0.0055	0.0095
naphthalene ( <b>1 h</b> )	0.0078	0.0126
3,4-dimethoxy ( <b>1 i</b> )	0.0047	0.0094
4-methoxy-3-methyl ( <b>1 j</b> )	0.0050	0.0093
3,4,5-trimethoxy ( <b>1 k</b> )	0.0036	0.0090
4-dimethylamino ( <b>1 l</b> )	0.0002	0.0009
2-chlorothiophene ( <b>2 a</b> )	0.0019	0.0030
thiophene ( <b>2 b</b> )	0.0022	0.0038
3-methylthiophene ( <b>2 c</b> )	0.0028	0.0041
2-methylthiophene ( <b>2 d</b> )	0.0029	0.0042
benzothiophene ( <b>2 e</b> )	0.0039	0.0046

[a] Calculated by using an appropriate fluorescence standard (1.0 μM sensor, 25 mM HEPES, 50 mM Na<sub>2</sub>S<sub>2</sub>O<sub>3</sub>, pH 5.0, 37 °C). [b] Excited at 473 nm. [c] Solutions contain 500 mM glutamate. [d] Benzene-based derivatives excited at 488 nm; thiophene-based derivatives excited at 515 nm. [e] Solution contained 5% DMSO. [f] Solution contained 30% DMSO.

**Table 2.** Association constants ( $K_a$ ) for the binding of the series 1 sensors to various analytes.<sup>[a]</sup>

Benzene-based moiety	Amine guest					
	Glutamate		Norepinephrine		Dopamine	
	$K_a$ [M <sup>-1</sup> ] <sup>[b]</sup>	$I_{sat}/I_0$ <sup>[c]</sup>	$K_a$ [M <sup>-1</sup> ] <sup>[b]</sup>	$I_{sat}/I_0$ <sup>[c]</sup>	$K_a$ [M <sup>-1</sup> ] <sup>[b]</sup>	$I_{sat}/I_0$ <sup>[c]</sup>
4-carbethoxy ( <b>1 a</b> ) <sup>[d]</sup>	7.0	4.7	81.5	1.8	107.5	1.1
phenyl ( <b>1 b</b> )	9.4	10.5	68.7	6.6	68.1	3.2
3-methyl ( <b>1 c</b> )	9.2	10.0	68.4	6.6	74.1	3.2
4-methylthio ( <b>1 d</b> )	8.4	9.8	68.8	6.5	87.1	3.1
4-biphenyl ( <b>1 e</b> ) <sup>[d]</sup>	13.8	6.2	148.8	2.6	203.3	1.6
3-fluoro-4-methoxy ( <b>1 f</b> )	9.0	9.3	70.2	6.4	92.9	3.1
(NS521) 4-methoxy ( <b>1 g</b> )	9.6	7.8	77.8	5.4	112.1	3.0
naphthalene ( <b>1 h</b> )	10.1	6.8	103.7	4.3	170.0	2.9
3,4-dimethoxy ( <b>1 i</b> )	10.2	6.6	107.2	4.1	177.5	2.7
4-methoxy-3-methyl ( <b>1 j</b> )	10.3	6.4	136.0	3.9	192.1	2.4
3,4,5-trimethoxy ( <b>1 k</b> )	10.3	5.6	159.1	2.6	205.1	1.6
4-dimethylamino ( <b>1 l</b> )	10.2	1.7	160.0	1.2	206.2	1.1

[a] Measured in buffer (1.0 μM sensor, 25 mM HEPES, 50 mM Na<sub>2</sub>S<sub>2</sub>O<sub>3</sub>, pH 5.0, 37 °C). [b]  $K_a$  measured by fluorescence spectroscopy. Excited at 488 nm. [c]  $I_{sat}$  = fluorescence intensity at saturation taken from the theoretical fit to a one-site binding isotherm. [d] Sensors **1 a** and **1 e** were adjusted to 5 and 30% DMSO, respectively.

## Discussion

### Binding affinity and selectivity

Glutamate binds to all derivatives with the same relatively low affinity (5–10 M<sup>-1</sup>). This result is consistent with other coumarin aldehyde sensors, which appear to bind all primary alkyl amines with similar low affinity.<sup>[7]</sup> Surprisingly, the catecholamines bind roughly an order of magnitude better. Moreover, there is a clear trend toward better binding to sensors with more electron-rich aromatic groups in position C4. There ap-

pears to be subtle interaction between the catechol group and the C4-aromatic, which increases with electron density on the C4-aromatic residue. Interestingly, the thiophene-based sensors demonstrated slightly lower overall affinity than the benzene-based sensors and the electronic structure of the thiophene does not appear to influence the binding constant of catecholamines. Although these binding constants are modest, they should suffice for cell imaging purposes because catecholamines are present at high concentrations (0.5–1 M) in secretory vesicles compared with the concentrations of typical free primary amines present in a cell (5 mM) and would promote binding. Indeed, even glutamate is thought to be present in concentrations as high as 300 mM in vesicles of glutamatergic neurons.<sup>[8b]</sup> Given that NS521 appears to accumulate in vesicles (vide supra), it is possible that some of the sensors described here could be used to image glutamate as well as catecholamines.

### Spectroscopic properties

Upon analyte addition, the fluorescence enhancements for the series 1 sensors were very good: as high as an elevenfold increase for glutamate and a 6.6-fold increase for norepinephrine. As the absorbance maximum shifts to the red upon interaction with the analyte, selective excitation of the red wavelength produces a fluorescence increase upon binding. In addition, the fluorescence quantum yields of the bound sensors were higher than those for the unbound sensors. Thus, the observed fluorescence enhancements are due to the selective excitation wavelength used and an increase in fluorescence quantum yield upon binding. Indeed, better enhancements might be possible by judicious choice of excitation wavelength; however, we chose to use 488 nm because this wavelength is commonly available for imaging applications. The catecholamines can quench by PET, which is reflected in a lower fluorescence quantum yield for the dopamine- and norepinephrine-bound sensors compared to sensors bound to glutamate. However, useful enhancements are seen even for those quenching analytes (Tables 2 and 3). It should be noted that sensors **1 a** and **1 e** required a DMSO co-solvent due to solubility issues, so the spectroscopic properties of these two sensors are not directly comparable to the others in this series and they would presumably not be compatible with cellular applications.

The fluorescence response of the series 2 sensors to the primary amine analytes was markedly higher than the fluorescence response of the series 1 sensors: as high as 57-fold for glutamate and 48-fold for norepinephrine. The difference in fluorescence response can be attributed to a lower initial fluorescence baseline. From Table 1, the quantum yields of the unbound thiophene derivatives are lower than those for the unbound benzene derivatives; however, the change in quantum yield between bound and unbound state were similar to the series 1 sensors. The major difference in the case of the

**Table 3.** Association constants ( $K_a$ ) for the binding of the series 2 sensors to various analytes.<sup>[a]</sup>

Thiophene-based moiety	Glutamate		Amine guest Norepinephrine		Dopamine	
	$K_a$ [ $M^{-1}$ ] <sup>[b]</sup>	$I_{sat}/I_0$ <sup>[c]</sup>	$K_a$ [ $M^{-1}$ ] <sup>[b]</sup>	$I_{sat}/I_0$ <sup>[c]</sup>	$K_a$ [ $M^{-1}$ ] <sup>[b]</sup>	$I_{sat}/I_0$ <sup>[c]</sup>
2-chlorothiophene ( <b>2a</b> )	5.9	34	69.2	21	84.0	12
(NS539) thiophene ( <b>2b</b> )	7.3	57	65.2	48	43.6	25
3-methylthiophene ( <b>2c</b> )	7.4	51	63.6	38	51.1	23
2-methylthiophene ( <b>2d</b> )	6.1	48	58.7	32	54.6	22
benzothiophene ( <b>2e</b> )	5.2	30	49.6	17	49.3	9.5

[a] Measured in buffer (5.0  $\mu M$  sensor, 25 mM HEPES, 50 mM  $Na_2S_2O_3$ , pH 5.0, 37 °C).  
 [b]  $K_a$  measured by fluorescence spectroscopy. Excited at 515 nm. [c]  $I_{sat}$  = fluorescence intensity at saturation taken from the theoretical fit to a one-site binding isotherm.

series 2 sensors is that they were excited at 515 nm to mimic a common laser line rather than exciting at the absorption maxima ( $\approx 502$  nm). At this higher excitation wavelength, the unbound derivative hardly absorbs, resulting in an overall low background that contributes to the very high fluorescence enhancements ( $I_{sat}/I_0$ ) seen in Table 3.

### Quantitative study of the PET process in series 1 sensors

Optimized models of the benzene-based sensors clearly indicate that the pendant aryl moiety is nearly perpendicular to the plane of the coumarin aldehyde scaffold (Figure 3). The modeling results are supported by the fact that all of the benzene-based sensors (except **1h**) have approximately the same absorbance and emission maxima, indicating that the ground-state interaction between the pendant aryl moiety and the coumarin aldehyde scaffold was similar in all of them. In all cases, dopamine and norepinephrine produced a lower fluorescence response than glutamate. Indeed, serotonin completely quenched the fluorescence response of all sensor derivatives upon binding (data not shown). The calculated  $E_{HOMO}$  values of the catecholamines and serotonin (Table S3 in the Supporting Information) indicate that these analytes should

act as PET quenchers, with serotonin being a stronger PET quencher than dopamine, which is stronger than norepinephrine. Indeed, this expectation was borne out from the observed fluorescence enhancements.

As can be seen in Table 1, a wide range of fluorescence quantum yields was observed with the more electron-rich pendant aryl moieties giving much stronger quenching. Interestingly, the quantum yields of the bound species are uniformly higher than the unbound species. The iminium ion formed upon binding is more electron-poor than the corresponding aldehyde and thus, should be subject to stronger quenching (i.e., lower quantum yield) by the C4-aromatic group. However, this quenching effect is more than offset by the formation of the iminium ion which stabilizes and rigidifies the ICT state, thereby resulting in an overall increase in quantum yield upon binding.

To evaluate the photophysical interaction between the pendant aryl moiety and the coumarin aldehyde scaffold, the relationship between the quantum yield for the unbound and bound series 1 sensors and the calculated  $E_{HOMO}$  values of the corresponding benzene moiety was plotted and fit to the Marcus equation on the basis of the calculated  $E_{HOMO}$  values (Figure 5). In theory, increased electron density of the derivative would lead to a more positive HOMO energy value, faster electron transfer, and by default, a lower quantum yield due to greater quenching.<sup>[3b,9]</sup> The calculated free energy change for electron transfer ( $\Delta G_{ET}$ ) values, a prerequisite for fluorescence analysis in terms of the Marcus theory, were obtained as per the Rehm–Weller equation (Supporting Information). In turn, the calculated free energy change for electron transfer ( $\Delta G_{ET}$ ) values were derived, in part, from the oxidation and reduction potential values using an established linear correlation between the molecular orbital energy values ( $E_{HOMO}$  and  $E_{LUMO}$ ) and the experimentally measured oxidation and reduction potential values.<sup>[10]</sup> The experimentally determined quantum yields aligned with the fitted curves quite well, indicating that the sensor platform fits the model of a directly linked donor–

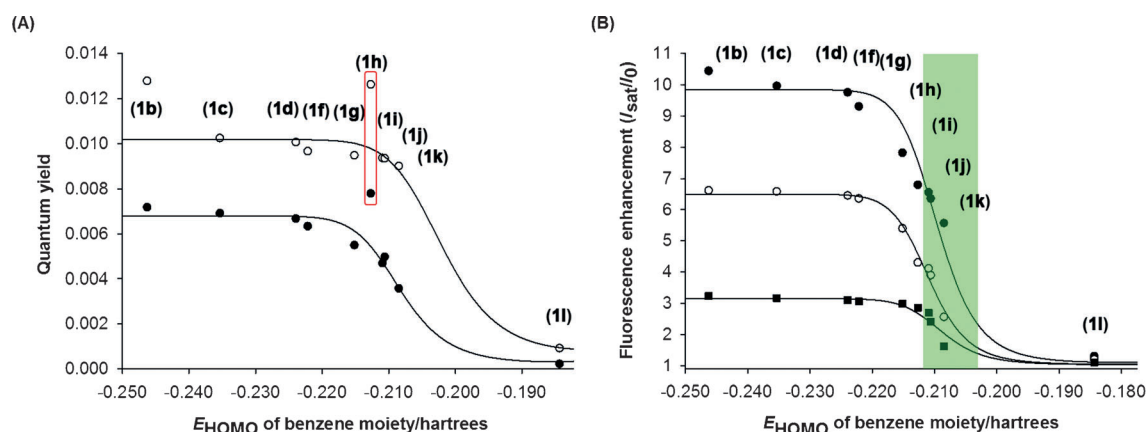


**Figure 5.** A) Relationship between the calculated  $E_{HOMO}$  values of the pendant aryl moiety and the fluorescence quantum yields for series 1 sensors (●) unbound and (○) bound with glutamate. The red box highlights naphthalene derivative. B) Relationship between the calculated  $E_{HOMO}$  values of the pendant aryl moiety and the fluorescence enhancement for series 1 sensors with (●) glutamate, (○) norepinephrine, and (■) dopamine. The shaded region identifies derivatives with selective fluorescent responses. The curves represent the best fit to the Marcus equation.

acceptor system. In the case of compound **1h** having the 1-naphthyl group, both the unbound and bound quantum yields of **1h** are higher than theory would predict. However, this difference is attributed to the greater rigidification of the fluorophore (vide infra) because the C4-naphthyl moiety is closer to 90° from the plane of the fluorophore (Figure 3).

Because the absorbance maxima of the series **1** sensors were similar in both unbound and bound forms, the differences in fluorescent enhancement ( $I_{\text{sat}}/I_0$ ) from Table 2 are due entirely to variations in quantum yield between the two forms. Thus, these maximum fluorescence changes were plotted versus the calculated  $E_{\text{HOMO}}$  values (Figure 5B) and the same trends were observed as when plotting just the quantum yield. Indeed, compound **1h**, which was an outlier in Figure 5A, falls in line with the other derivatives in such a plot, indicating that the effect of the naphthyl group on the quantum yield was similar in both the bound and unbound states. Interestingly, the fluorescence enhancement for the series **1** sensors toward glutamate, norepinephrine, and dopamine followed a similar relationship, indicating that quenching analytes such as dopamine can quench all the sensors to the same degree. From this type of analysis, it is possible to identify sensors that would give selective turn-on fluorescent responses. For example, compounds in the green region of Figure 5B should give a good response to glutamate, but much weaker response to dopamine and norepinephrine. Of the sensors tested here, compound **1k** appears to be the best glutamate-selective sensor. Taken together, these results support the notion that a PET process modulates the fluorescence properties of the sensor platform and establishes a method for the rational design of selective sensors for primary-amine neurotransmitters by variation of the C4-substituent.

### Variation in the quantum yields for the series 2 sensors

Calculations indicated that the thiophene substituents have more  $\pi$ -overlap with the fluorophore than the phenyl groups of the series **1** sensors. This overlap causes the absorbance and emission of the series **2** sensors to be at longer wavelengths. Indeed, the trends indicated that the more electron-rich thiophenes display higher wavelengths of excitation and emission. However, the quantum yields of the thiophene derivatives were lower than those of most of the series **1** sensors. This low-quantum-yield effect has been observed in other directly linked donor-acceptor systems (plat-

forms) and has sometimes been attributed to PET quenching from the thiophene.<sup>[11]</sup> For the series **2** sensors, the quantum yields trend upward as the group becomes more electron rich, thus an a-PET mechanism is not likely. It should be noted that for the chlorothiophene derivative (**2a**), it is possible that quenching due to the heavy atom effect of the chlorine may contribute to an anomalously low quantum yield for this sensor. Regardless, it is clear that PET quenching does not explain the low quantum yield of the thiophene derivatives.

If one compares the quantum yield of the naphthalene derivative (**1h**) to the other benzene derivatives (e.g., **1b**) and the thiophene derivatives (e.g., **2b**), the sensors in which the C4-group is more perpendicular, and thereby more rigid, have higher fluorescence quantum yields than those where the C4-group is more in plane with the coumarin aldehyde scaffold, and thereby less rigid (Figure 3). These results indicate that twisting of the aryl-fluorophore bond in the excited state leads to nonradiative decay processes and lowers the quantum yield of the fluorophore.<sup>[12,13]</sup>

### Summary of the fluorescence responses

The fluorescence enhancements for the series **1** and **2** sensors upon binding to glutamate, norepinephrine, and dopamine are summarized in Figure 6 and Figure 7, respectively. It should be noted that sensor **1g** (NS521) does not have the highest fluorescence response of the series **1** sensors. However, we chose to utilize sensor **1g** in our initial work because it struck a good balance between high fluorescence responses and good binding affinity toward norepinephrine and dopamine

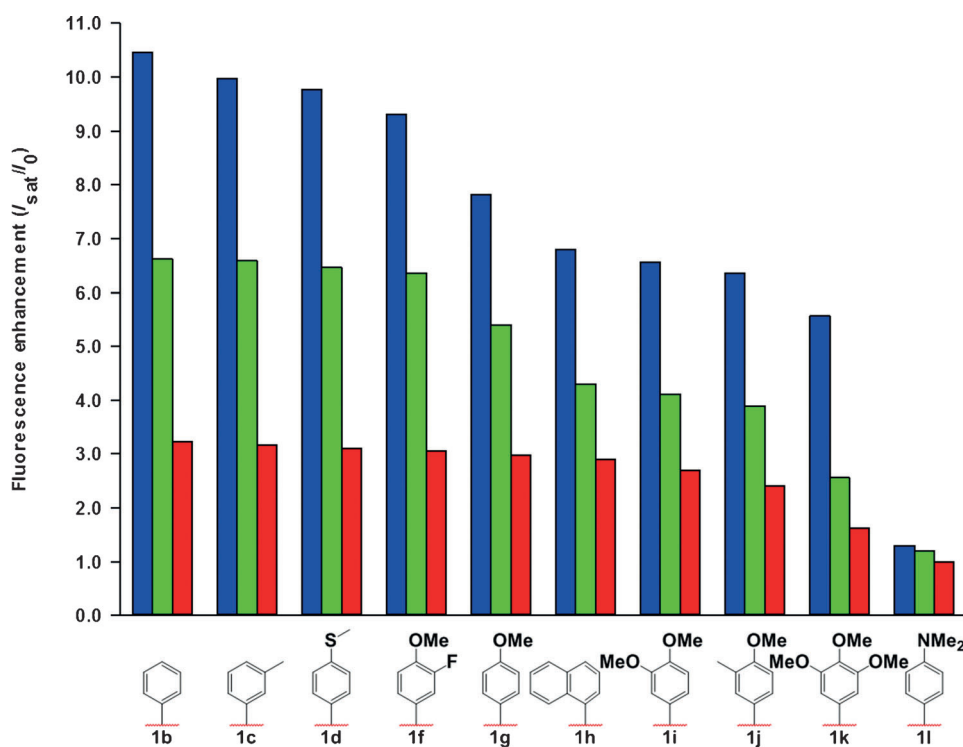
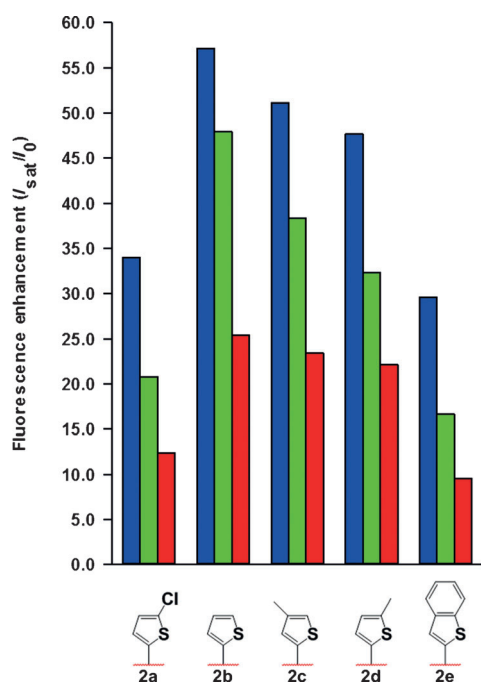


Figure 6. The fluorescence enhancements of series **1** derivatives toward glutamate (blue), norepinephrine (green), and dopamine (red).



**Figure 7.** The fluorescence enhancements of series 2 derivatives toward glutamate (blue), norepinephrine (green), and dopamine (red).

that would provide selective labeling and imaging in cellular studies. Overall, compared to the benzene-based series 1 sensors, the thiophene-based series 2 sensors provided only subtle differences in binding constants. However, the fluorescence enhancements for the thiophene-based series were considerably larger than the fluorescence enhancements for the benzene-based series. Of this series, sensor **2b** had the highest fluorescence enhancements due to a high ratio of quantum yields between the unbound and bound sensor as well as high

binding affinities toward the primary-amine analytes. Given the high fluorescence enhancements and redshifted fluorescence properties observed for compound **2b** (Table 3), we named this compound NeuroSensor 539 (NS539) and pursued cell imaging studies.

### Confocal fluorescence spectroscopy

Norepinephrine- and epinephrine-secreting chromaffin cells were isolated from bovine adrenal glands, separately incubated with NS539 (**2b**, 10  $\mu\text{M}$ ), and imaged using confocal fluorescence microscopy. The live cells were imaged at 458 nm which would excite any potential unbound sensor and at 514 nm which would excite the bound sensor. Excitation of the epinephrine cells at 514 nm provided marginal fluorescence response, indicating that the sensor is not binding to epinephrine (Figure 8B) as expected since epinephrine is a secondary-amine neurotransmitter (Figure 2).<sup>[6]</sup> The residual fluorescence signal could be attributed to incomplete conversion of norepinephrine to epinephrine by the phenylethanolamine *N*-methyltransferase (PNMT) enzyme, given that epinephrine-enriched chromaffin cells have been shown to contain 2–37% norepinephrine.<sup>[14]</sup> Excitation at 458 nm gave no fluorescence, indicating that the unbound neutral sensor does not remain inside the cell (Figure 8A). However, the norepinephrine-enriched cells exhibited strong punctate fluorescence upon excitation at 514 nm (Figure 8E). Exciting the norepinephrine-enriched cells at the wavelength associated with the unbound sensor ( $\lambda_{\text{ex}} = 458 \text{ nm}$ ) similarly provided no measurable fluorescence response (Figure 8D). The results indicate that the NS539 only accumulates within secretory vesicles upon binding to norepinephrine, as previously seen with NS521.<sup>[6]</sup> The ratio of the mean corrected total cell fluorescence intensity of norepinephrine- over epinephrine-enriched cells was approximately

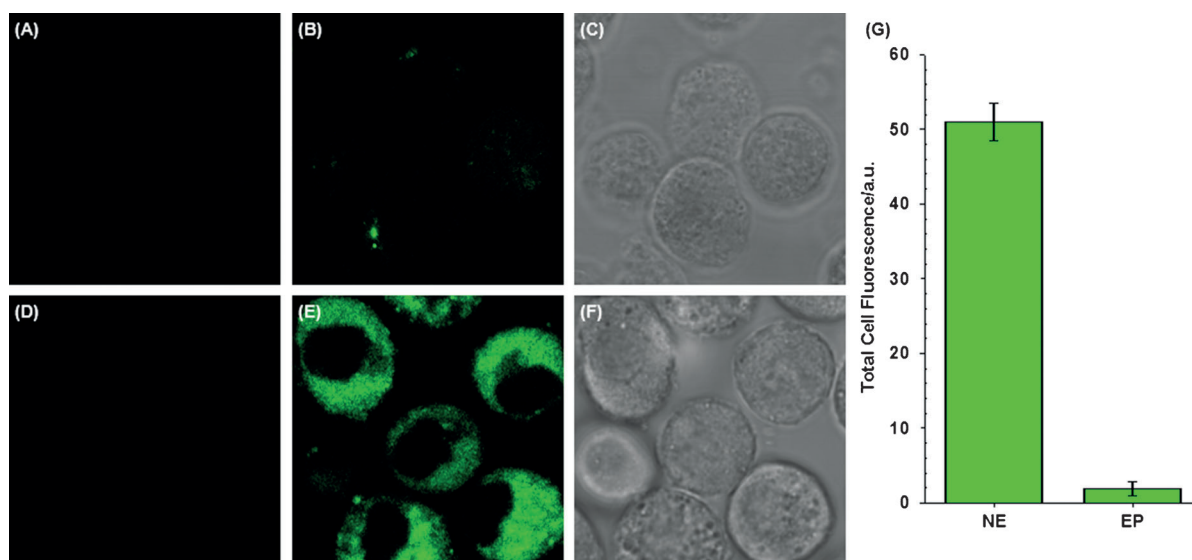


**Figure 8.** Epinephrine-enriched cells (vesicles contain 0.5–1.0 M epinephrine) incubated with NS539 (**2b**, 10  $\mu\text{M}$ ): A)  $\lambda_{\text{ex}} = 458 \text{ nm}$ , B)  $\lambda_{\text{ex}} = 514 \text{ nm}$ , C) brightfield image. Norepinephrine-enriched cells (vesicles contain 0.5–1.0 M norepinephrine) incubated with NS539 (**2b**, 10  $\mu\text{M}$ ): D)  $\lambda_{\text{ex}} = 458 \text{ nm}$ , E)  $\lambda_{\text{ex}} = 514 \text{ nm}$ , F) brightfield image. Fluorescence was visualized using a 535–590 nm bandpass filter. G) The mean corrected total cell fluorescence intensity for norepinephrine- and epinephrine-enriched (NE and EP, respectively) cells was  $51.0 \pm 2.6$  and  $1.86 \pm 0.98$  respectively. Error bars represent standard deviation ( $n = 6$ ).

27-fold (Figure 8G). These results validate NS539 as an excellent sensor for cellular imaging of primary-amine neurotransmitters with very low background.

## Conclusion

These data suggest that the coumarin-3-aldehyde scaffold and pendant aryl-based moiety comprise a platform that constitutes a new directly linked donor–acceptor system when the pendant aryl moiety is benzene-based and thus, perpendicular to the plane of the fluorophore. The benzene-substituted series of sensors operates through an a-PET mechanism, which allows one to predict both the fluorescence quantum yields and the fluorescence responses toward primary-amine neurotransmitters based on DFT calculations. The results provide a rational design strategy for the development of turn-on fluorescent sensors for primary-amine neurotransmitters based on the coumarin-3-aldehyde scaffold. The thiophene-substituted series of sensors did not follow the same trend based on PET quenching, indicating that the  $\pi$ -system of the thiophene is more conjugated with the  $\pi$ -system of the fluorophore. However, due to favorable excitation/emission profiles, the thiophene sensors gave far superior fluorescence enhancements upon binding analytes. Based on these studies, NeuroSensor 539 was identified as a good candidate for biological imaging studies by demonstrating enhanced spectral and photophysical properties. The efficacy of NeuroSensor 539 was validated by selectively labeling and imaging norepinephrine in secretory vesicles of live chromaffin cells using longer excitation wavelengths that provided lower background. Future considerations will include studying cell viability and the response of such sensors in tissues.

## Experimental Section

### Materials and general instrumentation

All chemicals were obtained from Acros Organics, Sigma–Aldrich, Alfa Aesar, Combi-Blocks, or Fisher Scientific and were used without further purification. Flash chromatography was performed with 32–63  $\mu\text{m}$  silica gel.  $^1\text{H}$  NMR and  $^{13}\text{C}$  NMR spectra were recorded on a Bruker DRX 500. IR spectra were recorded on a Nexus 670 FT-IR E.S.P. spectrometer. Distilled water was used to prepare all aqueous solutions.

### Computational methods

Conventional DFT calculations using the hybrid exchange–correlation function B3LYP with the 6–31G(d) basis set as implemented in Gaussian 09W Rev. A.02<sup>[16]</sup> were performed on the benzene- and thiophene-based coumarin-3-aldehyde derivatives in the gas phase. Several starting geometries were used for the geometry optimization to ensure that the optimized structure corresponds to a global minimum. The final optimized geometry was unaffected by the various initial starting geometries for each sensor.

### Fluorescence titrations

Fluorescence spectra were recorded on a Shimadzu RF-5301 PC spectrofluorometer at 37 °C. A separate 1 mg mL<sup>-1</sup> stock solution

of each coumarin-3-aldehyde derivative in DMSO was prepared. An aqueous stock solution of each derivative (10  $\mu\text{M}$ ) in buffer (25 mM HEPES, 50 mM Na<sub>2</sub>S<sub>2</sub>O<sub>3</sub>, pH 5.0) was prepared. Norepinephrine, dopamine, glutamate, and epinephrine stock solutions were prepared by separately dissolving the solid analytes at the concentration to be used in the titration with the buffered stock solutions described above and thus, avoiding dilution of the sensor during the experiment. The benzene-based NS521 derivatives were excited at 488 nm. The thiophene-based derivatives were excited at 515 nm.

### Fluorescence properties and quantum yields

Steady-state fluorescence spectroscopic studies were performed using a Horiba Scientific Fluorolog-3 Model FL3C-111 spectrofluorometer and data was collected and analyzed using HJY FluorEs-sence 3.5.1.20 software package. UV/Vis spectra were obtained on a Varian Cary 1E UV/Vis spectrophotometer. A stock solution of each benzene- or thiophene-based coumarin-3-aldehyde derivative (1  $\mu\text{M}$ ) in buffer (25 mM HEPES, 50 mM Na<sub>2</sub>S<sub>2</sub>O<sub>3</sub>, pH 5.0) was prepared. Each solution contained 1% (v/v) DMSO as a co-solvent except as noted. The slit width was 2 nm for both excitation and emission. The bound benzene- and thiophene-substituted coumarin-3-aldehyde derivatives contained 500 mM glutamate (pH 5.0).

To determine the relative quantum yield of fluorescence ( $\Phi_{\text{fl}}$ ) for the benzene-based derivatives, a 1.0  $\mu\text{M}$  solution of fluorescein (absolute  $\Phi_{\text{fl}}=0.85$ ) in 0.1 N NaOH (pH 13) was used as a fluorescence standard.<sup>[15]</sup> The unbound derivatives were excited at 473 nm and the bound derivatives were excited at 488 nm. To determine the relative quantum yield of fluorescence ( $\Phi_{\text{fl}}$ ) for the thiophene-based derivatives, a 1.0  $\mu\text{M}$  solution of rhodamine B (absolute  $\Phi_{\text{fl}}=0.31$ ) in water (pH 7) was used as a fluorescence standard.<sup>[17]</sup> The unbound derivatives were excited at 473 nm and the bound derivatives were excited at 515 nm. Quantum yields were obtained in triplicate and calculated as per the following Equation (1):

$$\Phi_{\text{S}} = \Phi_{\text{R}} \times \frac{I_{\text{S}}}{I_{\text{R}}} \times \frac{A_{\text{R}}}{A_{\text{S}}} \times \frac{n_{\text{S}}^2}{n_{\text{R}}^2} \quad (1)$$

in which  $\Phi_{\text{S}}$ =relative quantum yield of the sample,  $\Phi_{\text{R}}$ =absolute quantum yield of the reference,  $I_{\text{S}}$ =integrated fluorescence intensity of the sample,  $I_{\text{R}}$ =integrated fluorescence intensity of the reference,  $A_{\text{R}}$ =absorbance of the reference,  $A_{\text{S}}$ =absorbance of the sample,  $n_{\text{S}}$ =refractive index of the sample solvent, and  $n_{\text{R}}$ =refractive index of the reference solvent.

### Fluorescence imaging in live cells

Chromaffin cells were prepared as previously described.<sup>[8]</sup> Approximately 3 mL of each culture media containing suspended epinephrine- and norepinephrine-enriched cells was centrifuged at 1000 rpm for 5 min. The pellets were suspended in Dulbecco's Modified Eagle Medium (2 mL, DMEM). NS539 was added (10  $\mu\text{M}$  final concentration) and each cell suspension containing sensor incubated at 37 °C for 30 min. The cells were centrifuged, the supernatant removed, and washed twice with PBS buffer. Next, the cells were taken up into 6 mL standard cell bath solution and plated onto No. 1.5  $\gamma$ -irradiated poly-D-lysine coated 35 mm glass-bottom dishes (MatTek Corporation). The cells incubated on the dishes 37 °C with 5% CO<sub>2</sub> for 1 h prior to imaging to promote adhesion. Live cell imaging studies were performed using a Zeiss LSM 510 META laser scanning confocal microscope (Carl Zeiss Microscopy, LLC) equipped with a C-Apochromat 63x/1.2 water immersion objective lens (Carl Zeiss Microscopy, LLC). The excitation wave-

lengths were 458 and 514 nm (pixel time: 6.4  $\mu$ s, detector gain: 845, amplifier gain: 1.00, amplifier offset: -0.05, pinhole: 328  $\mu$ m). Image acquisition was performed using Zeiss AIM 4.2 software package (Carl Zeiss Microscopy, LLC). To compare the fluorescence intensities of the norepinephrine- versus the epinephrine-enriched cells, the mean corrected total cell fluorescence intensities were obtained using ImageJ (National Institute of Health).

### General procedure for synthesis of sensors 1a–l and 2e

Compound **3** (0.250 g, 0.894 mmol), arylboronic acid **4a–l** or **6e** (0.983 mmol), bis(dibenzylideneacetone)-palladium(0) (0.041 g, 0.045 mmol), 2-dicyclohexylphosphino-2',6'-dimethoxybiphenyl (SPhos) (0.055 g, 0.134 mmol), tribasic potassium phosphate (0.381 g, 1.788 mmol) were added to a flame-dried round bottom flask and flushed with N<sub>2</sub> for 30 min. Degassed THF (distilled, 6 mL) was added and the mixture stirred at 60 °C for 12–24 h under N<sub>2</sub>. The mixture was allowed to cool to room temperature, filtered through paper, rinsed with acetone, and the solvent removed in vacuo. The crude residue was purified by silica gel flash chromatography (100% CH<sub>2</sub>Cl<sub>2</sub>→80:20 CH<sub>2</sub>Cl<sub>2</sub>/EtOAc as eluent). The material was further purified by silica gel flash chromatography (90:10→50:50 hexanes/EtOAc as eluent) to afford compounds **1a–l** and **2e** as yellow oils.

**1a**: Yield: 83%. <sup>1</sup>H NMR (500 MHz, CDCl<sub>3</sub>):  $\delta$  = 9.95 (s, 1H), 8.18 (d, 2H, *J* = 8.0 Hz), 7.32 (d, 2H, *J* = 8.5 Hz), 6.84 (d, 1H, *J* = 9.0 Hz), 6.52 (d, 1H, *J* = 2.5 Hz), 6.49 (dd, 1H, *J* = 9.0, 2.5 Hz), 4.43 (q, 2H, *J* = 7.0 Hz), 3.45 (q, 4H, *J* = 7.5 Hz), 1.43 (t, 3H, *J* = 7.0 Hz), 1.23 ppm (t, 6H, *J* = 7.0 Hz); <sup>13</sup>C NMR (125 MHz, CDCl<sub>3</sub>):  $\delta$  = 188.0, 166.0, 160.5, 159.7, 157.8, 153.1, 138.3, 130.9, 130.8, 129.6, 128.1, 111.7, 109.9, 108.8, 97.1, 61.2, 45.2, 14.3, 12.4 ppm; IR (neat, cm<sup>-1</sup>):  $\tilde{\nu}$  = 2978, 1716, 1614, 1556, 1499, 1356, 1270, 1127, 1103, 727; HRMS Elemental analysis calcd (%) for C<sub>23</sub>H<sub>23</sub>NO<sub>5</sub>Na [*M*+Na<sup>+</sup>]: 416.1468; found: 416.1464.

**1b**: Yield: 64%. <sup>1</sup>H NMR (500 MHz, CD<sub>2</sub>Cl<sub>2</sub>):  $\delta$  = 9.78 (s, 1H), 7.47–7.55 (m, 3H), 7.23–7.30 (m, 2H), 6.93 (d, 1H, *J* = 10.0 Hz), 6.50–6.57 (m, 2H), 3.45 (q, 4H, *J* = 7.0 Hz), 1.23 ppm (t, 6H, *J* = 7.0 Hz); <sup>13</sup>C NMR (125 MHz, CD<sub>2</sub>Cl<sub>2</sub>):  $\delta$  = 188.4, 162.0, 159.9, 158.1, 153.4, 133.7, 131.2, 129.3, 128.8, 128.7, 112.7, 110.2, 109.5, 97.4, 45.6, 12.5 ppm; IR (neat, cm<sup>-1</sup>):  $\tilde{\nu}$  = 2974, 1751, 1715, 1683, 1617, 1559, 1504, 1418, 1354; HRMS Elemental analysis calcd (%) for C<sub>20</sub>H<sub>19</sub>NO<sub>3</sub>Na [*M*+Na<sup>+</sup>]: 344.1257; found: 344.1254.

**1c**: Yield: 82%. <sup>1</sup>H NMR (500 MHz, CDCl<sub>3</sub>):  $\delta$  = 9.79 (s, 1H), 7.39 (t, 1H, *J* = 8.0 Hz), 7.31 (d, 1H, *J* = 8.0 Hz), 7.06–7.09 (m, 2H), 6.98 (d, 1H, *J* = 10.0 Hz), 6.48–6.53 (m, 2H), 3.43 (q, 4H, *J* = 7.0 Hz), 2.42 (s, 3H), 1.22 ppm (t, 6H, *J* = 7.0 Hz); <sup>13</sup>C NMR (125 MHz, CDCl<sub>3</sub>):  $\delta$  = 188.4, 162.6, 159.4, 157.7, 153.0, 138.2, 132.8, 131.0, 129.9, 129.0, 128.3, 125.6, 112.3, 109.6, 109.0, 97.0, 45.1, 21.4, 12.4 ppm; IR (neat, cm<sup>-1</sup>):  $\tilde{\nu}$  = 1744, 1712, 1614, 1556, 1503, 1417, 1352, 1127, 730; HRMS Elemental analysis calcd (%) for C<sub>21</sub>H<sub>21</sub>NO<sub>3</sub>Na [*M*+Na<sup>+</sup>]: 358.1414; found: 358.1413.

**1d**: Yield: 36%. <sup>1</sup>H NMR (500 MHz, CDCl<sub>3</sub>):  $\delta$  = 9.88 (s, 1H), 7.36 (d, 2H, *J* = 8.5 Hz), 7.20 (d, 2H, *J* = 8.5 Hz), 7.01 (d, 1H, *J* = 8.0 Hz), 6.48–6.52 (m, 2H), 3.45 (q, 4H, *J* = 7.0 Hz), 2.56 (s, 3H), 1.24 ppm (t, 6H, *J* = 7.0); <sup>13</sup>C NMR (125 MHz, CDCl<sub>3</sub>):  $\delta$  = 188.3, 161.3, 159.9, 157.8, 153.0, 140.5, 130.9, 129.3, 129.0, 125.7, 112.3, 109.6, 109.0, 97.1, 45.2, 15.3, 12.4 ppm; IR (neat, cm<sup>-1</sup>):  $\tilde{\nu}$  = 1746, 1714, 1612, 1558, 1507, 1487, 1420, 1353, 1132; HRMS Elemental analysis calcd (%) for C<sub>21</sub>H<sub>21</sub>NO<sub>3</sub>Na [*M*+Na<sup>+</sup>]: 390.1134; found: 390.1132.

**1e**: Yield: 25%. <sup>1</sup>H NMR (500 MHz, CDCl<sub>3</sub>):  $\delta$  = 9.92 (s, 1H), 7.74 (d, 2H, *J* = 8.5 Hz), 7.68 (d, 2H, *J* = 8.0 Hz), 7.50 (t, 2H, *J* = 7.5 Hz), 7.42 (t, 1H, *J* = 7.5 Hz), 7.36 (d, 2H, *J* = 8.0 Hz), 7.06 (d, 1H, *J* = 9.5 Hz), 6.51–6.56 (m, 2H), 3.45 (q, 4H, *J* = 7.5 Hz), 1.26 ppm (t, 6H, *J* =

7.5 Hz); <sup>13</sup>C NMR (125 MHz, CDCl<sub>3</sub>):  $\delta$  = 188.4, 161.7, 159.8, 157.8, 153.1, 142.0, 140.1, 131.9, 131.0, 129.0, 128.9, 127.8, 127.2, 127.1, 112.4, 109.7, 109.1, 97.1, 45.2, 12.4 ppm; IR (neat, cm<sup>-1</sup>):  $\tilde{\nu}$  = 1745, 1711, 1610, 1558, 1498, 1419, 1352, 1131; HRMS Elemental analysis calcd (%) for C<sub>26</sub>H<sub>23</sub>NO<sub>3</sub>Na [*M*+Na<sup>+</sup>]: 420.1570; found: 420.1568.

**1f**: Yield: 69%. <sup>1</sup>H NMR (500 MHz, CDCl<sub>3</sub>):  $\delta$  = 9.91 (s, 1H), 7.09 (t, 1H, *J* = 8.5 Hz), 6.98–7.03 (m, 3H), 6.49–6.55 (m, 2H), 3.98 (s, 3H), 3.46 (q, 4H, *J* = 7.0 Hz), 1.22 ppm (t, 6H, *J* = 7.0 Hz); <sup>13</sup>C NMR (125 MHz, CDCl<sub>3</sub>):  $\delta$  = 188.2, 160.1, 159.8, 157.8, 153.0, 152.9, 151.0, 148.4, 148.3, 130.8, 125.5, 125.4, 124.8, 116.6 (C-F, d, *J* = 20.0 Hz), 113.2, 113.1, 112.2, 109.8, 109.0, 97.1, 56.3, 45.2, 12.4 ppm; IR (neat, cm<sup>-1</sup>):  $\tilde{\nu}$  = 1747, 1614, 1556, 1520, 1499, 1429, 1417, 1354, 1270, 1136; HRMS Elemental analysis calcd (%) for C<sub>21</sub>H<sub>20</sub>FNO<sub>4</sub>Na [*M*+Na<sup>+</sup>]: 392.1268; found: 392.1267.

**1h**: Yield: 67%. <sup>1</sup>H NMR (500 MHz, CDCl<sub>3</sub>):  $\delta$  = 9.72 (s, 1H), 7.98 (d, 1H, *J* = 8.5 Hz), 7.94 (dd, 1H, *J* = 8.5, 1.5 Hz), 7.58 (t, 1H, *J* = 7.5 Hz), 7.48–7.54 (m, 2H), 7.41 (td, 1H, *J* = 8.0, 1.0 Hz), 7.34 (dd, 1H, *J* = 7.0, 1.0 Hz), 6.70 (d, 1H, *J* = 9.0), 6.55 (d, 1H, *J* = 2.5 Hz), 6.37 (dd, 1H, *J* = 9.5, 2.5 Hz), 3.42 (q, 4H, *J* = 7.0 Hz), 1.21 ppm (t, 6H, *J* = 7.0 Hz); <sup>13</sup>C NMR (125 MHz, CDCl<sub>3</sub>):  $\delta$  = 188.0, 161.1, 159.7, 153.2, 133.2, 131.1, 131.0, 130.9, 129.3, 128.5, 127.1, 126.5, 126.0, 125.1, 125.0, 113.3, 109.8, 109.5, 96.9, 45.2, 12.4 ppm; IR (neat, cm<sup>-1</sup>):  $\tilde{\nu}$  = 1744, 1716, 1679, 1614, 1552, 1499, 1417, 1352, 1136; HRMS Elemental analysis calcd (%) for C<sub>24</sub>H<sub>21</sub>NO<sub>3</sub>Na [*M*+Na<sup>+</sup>]: 394.1414; found: 394.1413.

**1i**: Yield: 77%. <sup>1</sup>H NMR (500 MHz, CDCl<sub>3</sub>):  $\delta$  = 9.82 (s, 1H), 7.08 (d, 1H, *J* = 9.0 Hz), 7.00 (d, 1H, *J* = 8.0 Hz), 6.87 (dd, 1H, *J* = 8.0, 2.0 Hz), 6.80 (d, 1H, *J* = 1.5 Hz), 6.50–6.55 (m, 2H), 3.97 (s, 3H), 3.88 (s, 3H), 3.46 (q, 4H, *J* = 7.0 Hz), 1.25 ppm (t, 6H, *J* = 7.0 Hz); <sup>13</sup>C NMR (125 MHz, CDCl<sub>3</sub>):  $\delta$  = 188.5, 162.2, 159.4, 157.7, 153.0, 149.8, 148.9, 130.9, 125.0, 121.6, 112.6, 111.9, 110.9, 109.6, 109.1, 97.1, 56.1, 56.0, 45.2, 12.4 ppm; IR (neat, cm<sup>-1</sup>):  $\tilde{\nu}$  = 2974, 1736, 1650, 1615, 1506, 1455, 1377, 1168; HRMS Elemental analysis calcd (%) for C<sub>22</sub>H<sub>23</sub>NO<sub>3</sub>Na [*M*+Na<sup>+</sup>]: 404.1468; found: 404.1465.

**1j**: Yield: 54%. <sup>1</sup>H NMR (500 MHz, CDCl<sub>3</sub>):  $\delta$  = 9.75 (s, 1H), 7.03–7.10 (m, 3H), 6.91 (d, 1H, *J* = 8.5 Hz), 6.50 (dd, 1H, *J* = 8.5, 2.0 Hz), 6.48 (d, 1H, *J* = 2.0 Hz), 3.89 (s, 3H), 3.43 (q, 4H, *J* = 7.0 Hz), 2.25 (s, 3H), 1.21 ppm (t, 6H, *J* = 7.0 Hz); <sup>13</sup>C NMR (125 MHz, CDCl<sub>3</sub>):  $\delta$  = 188.6, 162.8, 159.2, 158.6, 157.6, 152.9, 131.1, 130.9, 127.8, 126.8, 124.0, 112.5, 109.5, 109.4, 109.0, 96.9, 55.4, 45.1, 16.2, 12.4 ppm; IR (neat, cm<sup>-1</sup>):  $\tilde{\nu}$  = 1746, 1611, 1511, 1495, 1419, 1353, 1251, 1137; HRMS Elemental analysis calcd (%) for C<sub>22</sub>H<sub>23</sub>NO<sub>4</sub>Na [*M*+Na<sup>+</sup>]: 388.1519; found: 388.1518.

**1k**: Yield: 37%. <sup>1</sup>H NMR (500 MHz, CDCl<sub>3</sub>):  $\delta$  = 9.81 (s, 1H), 7.08 (d, 1H, *J* = 9.0 Hz), 6.55 (dd, 1H, *J* = 9.0, 2.5 Hz), 6.52 (d, 1H, *J* = 2.5 Hz), 6.51 (s, 2H), 3.94 (s, 3H), 3.86 (s, 6H), 3.46 (q, 4H, *J* = 7.0 Hz), 1.24 ppm (t, 6H, *J* = 7.0 Hz); <sup>13</sup>C NMR (125 MHz, CDCl<sub>3</sub>):  $\delta$  = 188.3, 162.3, 159.1, 157.7, 153.4, 138.5, 130.8, 128.2, 112.4, 109.7, 108.8, 105.9, 97.0, 61.1, 56.3, 45.2, 12.4 ppm; IR (neat, cm<sup>-1</sup>):  $\tilde{\nu}$  = 1748, 1618, 1495, 1417, 1352, 1123; HRMS Elemental analysis calcd (%) for C<sub>23</sub>H<sub>25</sub>NO<sub>6</sub>Na [*M*+Na<sup>+</sup>]: 434.1574; found: 434.1570.

**1l**: Yield: 10%. <sup>1</sup>H NMR (500 MHz, CDCl<sub>3</sub>):  $\delta$  = 9.77 (s, 1H), 7.24 (d, 1H, *J* = 8.0 Hz), 7.21 (d, 2H, *J* = 7.0 Hz), 6.79 (d, 2H, *J* = 9.0 Hz), 6.49–6.54 (m, 2H), 3.45 (q, 4H, *J* = 7.0 Hz), 3.07 (s, 6H), 1.23 ppm (t, 6H, *J* = 7.0 Hz); <sup>13</sup>C NMR (125 MHz, CDCl<sub>3</sub>):  $\delta$  = 199.9, 163.4, 159.3, 157.7, 152.7, 151.2, 131.0, 130.9, 119.1, 112.5, 111.3, 109.3, 109.1, 97.1, 45.1, 40.2, 12.5 ppm; IR (neat, cm<sup>-1</sup>):  $\tilde{\nu}$  = 1743, 1610, 1558, 1496, 1418, 1355, 1132; HRMS Elemental analysis calcd (%) for C<sub>22</sub>H<sub>24</sub>N<sub>2</sub>O<sub>3</sub>Na [*M*+Na<sup>+</sup>]: 365.1860; found: 365.1860.

**2e**: Yield: 89%. <sup>1</sup>H NMR (500 MHz, CDCl<sub>3</sub>):  $\delta$  = 9.99 (s, 1H), 7.88 (dd, 1H, *J* = 8.5, 1.5 Hz), 7.85 (dd, 1H, *J* = 7.0, 2.0 Hz), 7.40–7.48 (m, 2H), 7.35 (s, 1H), 7.29 (d, 1H, *J* = 9.0 Hz), 6.50–6.56 (m, 2H), 3.46 (q, 4H,

$J=7.0$  Hz), 1.24 ppm (t, 6H,  $J=7.0$  Hz);  $^{13}\text{C}$  NMR (125 MHz,  $\text{CDCl}_3$ ):  $\delta=187.7, 159.2, 157.5, 154.3, 153.2, 140.7, 139.2, 132.9, 130.7, 126.1, 125.3, 125.0, 124.2, 122.2, 113.2, 109.9, 109.0, 97.0, 45.2, 12.4$ ; IR (neat,  $\text{cm}^{-1}$ ):  $\tilde{\nu}=1742, 1615, 1491, 1418, 1356, 1268, 1148, 723$  ppm; HRMS Elemental analysis calcd (%) for  $\text{C}_{22}\text{H}_{19}\text{NO}_3\text{SNa}$  [ $M+\text{Na}^+$ ]: 400.0978; found: 400.0977.

### General procedure for synthesis of precursors 7a–d

Compound **5** (250.0 mg, 1.072 mmol), *p*-toluenesulfonyl chloride (224.8 mg, 1.179 mmol), and  $\text{Na}_2\text{CO}_3$  (340.8 mg, 3.215 mmol) were added to a flame-dried round bottom flask and flushed with  $\text{N}_2$  for 15 min. Degassed  $\text{H}_2\text{O}/\text{THF}$  (1:20, 15.0 mL) was added and the mixture stirred at  $50^\circ\text{C}$  for 30 min. The mixture was allowed to cool to room temperature. Thiophene-based boronic acid **6a–d** (1.179 mmol) was added to the mixture and was allowed to stir at room temperature for 5 min. Palladium chloride (9.5 mg, 0.054 mmol) was added and the mixture stirred at  $50^\circ\text{C}$  for 6 h. The mixture was filtered through paper and the solvent removed in vacuo. The remaining residue was purified by chromatography (100%  $\text{CH}_2\text{Cl}_2 \rightarrow 95:5$   $\text{CH}_2\text{Cl}_2/\text{EtOAc}$  as eluent). The material was further purified by chromatography (90:10  $\rightarrow$  50:50 hexanes/ $\text{EtOAc}$  as eluent) to afford the compounds **7a–d** as pale yellow oils.

**7a**: Yield: 26%.  $^1\text{H}$  NMR (500 MHz,  $\text{CDCl}_3$ ):  $\delta=7.64$  (d, 1H,  $J=9.0$  Hz), 7.16 (d, 1H,  $J=4.0$  Hz), 7.01 (d, 1H,  $J=4.0$  Hz), 6.58 (dd, 1H,  $J=9.0, 2.5$  Hz), 6.55 (d, 1H,  $J=2.5$  Hz), 6.07 (s, 1H), 3.43 (q, 4H,  $J=7.0$  Hz), 1.22 ppm (t, 6H,  $J=7.0$  Hz);  $^{13}\text{C}$  NMR (125 MHz,  $\text{CDCl}_3$ ):  $\delta=161.6, 156.8, 150.8, 147.1, 135.6, 132.6, 128.0, 127.2, 126.9, 108.7, 108.1, 106.7, 98.0, 44.8, 12.4$  ppm; IR (neat,  $\text{cm}^{-1}$ ):  $\tilde{\nu}=2974, 1712, 1614, 1585, 1516, 1434, 1352, 1266, 1103$ ; HRMS Elemental analysis calcd (%) for  $\text{C}_{17}\text{H}_{16}\text{ClNO}_2\text{SNa}$  [ $M+\text{Na}^+$ ]: 356.0482; found: 356.0481.

**7b**: Yield: 23%.  $^1\text{H}$  NMR (500 MHz,  $\text{CDCl}_3$ ):  $\delta=7.69$  (d, 1H,  $J=8.5$  Hz), 7.51 (dd, 1H,  $J=5.5, 0.5$  Hz), 7.39 (dd, 1H,  $J=3.5, 0.5$  Hz), 7.18–7.21 (m, 1H), 6.55–6.61 (m, 2H), 6.15 (s, 1H), 3.44 (q, 4H,  $J=7.0$  Hz), 1.23 ppm (t, 6H,  $J=7.0$  Hz);  $^{13}\text{C}$  NMR (125 MHz,  $\text{CDCl}_3$ ):  $\delta=161.8, 156.8, 150.7, 148.2, 137.2, 128.6, 127.8, 127.7, 127.6, 108.6, 108.2, 107.1, 98.0, 44.8, 12.4$  ppm; IR (neat,  $\text{cm}^{-1}$ ):  $\tilde{\nu}=3101, 2974, 1704, 1614, 1430, 1405, 1352, 1274, 1107$ ; HRMS Elemental analysis calcd (%) for  $\text{C}_{17}\text{H}_{17}\text{NO}_2\text{SNa}$  [ $M+\text{Na}^+$ ]: 322.0872; found: 322.0871.

**7c**: Yield: 42%.  $^1\text{H}$  NMR (500 MHz,  $\text{CDCl}_3$ ):  $\delta=7.73$  (d, 1H,  $J=9.0$  Hz), 7.20 (s, 1H), 7.09 (s, 1H), 6.60 (dd, 1H,  $J=9.0, 3.0$  Hz), 6.57 (d, 1H,  $J=2.5$  Hz), 6.13 (s, 1H), 3.44 (q, 4H,  $J=7.0$  Hz), 2.35 (s, 3H), 1.23 ppm (t, 6H,  $J=7.0$  Hz);  $^{13}\text{C}$  NMR (125 MHz,  $\text{CDCl}_3$ ):  $\delta=161.9, 156.8, 150.7, 148.4, 138.5, 137.0, 130.9, 127.6, 123.3, 108.5, 107.9, 107.2, 98.0, 44.8, 15.8, 12.5$  ppm; IR (neat,  $\text{cm}^{-1}$ ):  $\tilde{\nu}=2921, 1708, 1610, 1584, 1516, 1409, 1352, 1099$ ; HRMS Elemental analysis calcd (%) for  $\text{C}_{18}\text{H}_{19}\text{NO}_2\text{SNa}$  [ $M+\text{Na}^+$ ]: 336.1029; found: 336.1029.

**7d**: Yield: 22%.  $^1\text{H}$  NMR (500 MHz,  $\text{CDCl}_3$ ):  $\delta=7.75$  (d, 1H,  $J=9.0$  Hz), 7.21 (d, 1H,  $J=3.5$  Hz), 6.85 (dd, 1H,  $J=2.5, 1.0$  Hz), 6.58 (dd, 1H,  $J=9.0, 2.5$  Hz), 6.56 (d, 1H,  $J=2.5$  Hz), 6.11 (s, 1H), 3.43 (q, 4H,  $J=7.0$  Hz), 2.57 (s, 3H), 1.22 ppm (t, 6H,  $J=7.0$  Hz);  $^{13}\text{C}$  NMR (125 MHz,  $\text{CDCl}_3$ ):  $\delta=162.0, 156.8, 150.6, 148.3, 143.0, 134.8, 128.9, 127.6, 126.2, 108.5, 107.5, 107.1, 98.0, 44.8, 15.4, 12.5$  ppm; IR (neat,  $\text{cm}^{-1}$ ):  $\tilde{\nu}=2970, 1712, 1610, 1585, 1409, 1352, 1107$ ; HRMS Elemental analysis calcd (%) for  $\text{C}_{18}\text{H}_{19}\text{NO}_2\text{SNa}$  [ $M+\text{Na}^+$ ]: 336.1029; found: 336.1026.

### General procedure for synthesis of sensors 2a–d

$\text{POCl}_3$  (5.2 mL, 56.1 mmol) was added to DMF (10.8 mL, 139.5 mmol) at  $0^\circ\text{C}$  in a flame-dried round bottom flask. The Vilsmeier reagent was stirred at ambient temperature for 45 min. The

Vilsmeier reagent (5 mL) was added to a solution **7a–d** in DMF (1 mL). The solution was stirred at ambient temperature for 12 h. The resulting red solution was poured onto cold  $\text{H}_2\text{O}$  (100 mL), basified with saturated  $\text{NaHCO}_3$  (50 mL), and extracted with  $\text{CH}_2\text{Cl}_2$  (100 mL  $\times$  3). The combined organic layers were dried over  $\text{Na}_2\text{SO}_4$  and the solvent was removed in vacuo. The residue was purified by chromatography (90:10  $\rightarrow$  50:50 hexanes/ $\text{EtOAc}$ ) to afford the desired formylated derivatives **2a–d** as yellow oils.

**2a**: Yield: 78%.  $^1\text{H}$  NMR (500 MHz,  $\text{CDCl}_3$ ):  $\delta=10.00$  (s, 1H), 7.30 (d, 1H,  $J=9.5$  Hz), 7.02 (d, 1H,  $J=4.0$  Hz), 6.89 (d, 1H,  $J=4.0$  Hz), 6.57 (dd, 1H,  $J=9.0, 2.5$  Hz), 6.49 (d, 1H,  $J=2.5$  Hz), 3.47 (q, 4H,  $J=7.0$  Hz), 1.24 ppm (t, 6H,  $J=7.0$  Hz);  $^{13}\text{C}$  NMR (125 MHz,  $\text{CDCl}_3$ ):  $\delta=187.7, 159.6, 157.5, 153.2, 152.4, 133.1, 131.1, 130.5, 128.8, 126.4, 113.2, 110.0, 109.1, 97.1, 45.2, 12.4$  ppm; IR (neat,  $\text{cm}^{-1}$ ) 2970, 1748, 1717, 1611, 1559, 1499, 1439, 1412; HRMS Elemental analysis calcd (%) for  $\text{C}_{18}\text{H}_{16}\text{ClNO}_3\text{SNa}$  [ $M+\text{Na}^+$ ]: 384.0432; found: 384.0432.

**2b**: Yield: 54%.  $^1\text{H}$  NMR (500 MHz,  $\text{CD}_2\text{Cl}_2$ ):  $\delta=9.84$  (s, 1H), 7.64 (dd, 1H,  $J=5.0, 1.0$  Hz), 7.20–7.25 (m, 2H), 7.16 (dd, 1H,  $J=4.0, 1.0$  Hz), 6.60 (dd, 1H,  $J=9.0, 2.5$  Hz), 6.53 (d, 1H,  $J=2.5$  Hz), 3.46 (q, 4H,  $J=7.5$  Hz), 1.23 ppm (t, 6H,  $J=7.5$  Hz);  $^{13}\text{C}$  NMR (125 MHz,  $\text{CD}_2\text{Cl}_2$ ):  $\delta=188.0, 159.2, 157.9, 155.0, 153.5, 132.7, 130.9, 130.2, 128.7, 127.7, 114.0, 110.4, 109.8, 97.5, 45.7, 12.6$  ppm; IR (neat,  $\text{cm}^{-1}$ ):  $\tilde{\nu}=2921, 1740, 1614, 1495, 1442, 1417, 1356$ ; HRMS Elemental analysis calcd (%) for  $\text{C}_{18}\text{H}_{17}\text{NO}_3\text{SNa}$  [ $M+\text{Na}^+$ ]: 350.0821; found: 350.0818.

**2c**: Yield: 72%.  $^1\text{H}$  NMR (500 MHz,  $\text{CDCl}_3$ ):  $\delta=9.89$  (s, 1H), 7.34 (d, 1H,  $J=8.5$  Hz), 7.19 (s, 1H), 6.97 (s, 1H), 6.57 (dd, 1H,  $J=9.0, 2.5$  Hz), 6.50 (d, 1H,  $J=2.5$  Hz), 3.46 (q, 4H,  $J=7.0$  Hz), 2.36 (s, 3H), 1.25 ppm (t, 6H,  $J=7.0$  Hz);  $^{13}\text{C}$  NMR (125 MHz,  $\text{CDCl}_3$ ):  $\delta=188.0, 158.8, 157.5, 155.3, 153.1, 138.1, 132.3, 131.8, 130.6, 124.0, 113.5, 109.7, 109.1, 97.1, 45.2, 15.6, 12.5$  ppm; IR (neat,  $\text{cm}^{-1}$ ):  $\tilde{\nu}=2966, 1748, 1712, 1610, 1438, 1373, 1270, 1070, 731$ ; HRMS Elemental analysis calcd (%) for  $\text{C}_{19}\text{H}_{19}\text{NO}_3\text{SNa}$  [ $M+\text{Na}^+$ ]: 364.0978; found: 364.0977.

**2d**: Yield: 83%.  $^1\text{H}$  NMR (500 MHz,  $\text{CDCl}_3$ ):  $\delta=9.92$  (s, 1H), 7.41 (d, 1H,  $J=9.5$  Hz), 6.99 (d, 1H,  $J=3.5$  Hz), 6.88 (dd, 1H,  $J=3.5, 1.0$  Hz), 6.58 (dd, 1H,  $J=9.0, 2.5$  Hz), 6.52 (d, 1H,  $J=2.5$  Hz), 3.48 (q, 4H,  $J=7.0$  Hz), 2.61 (s, 3H), 1.26 ppm (t, 6H,  $J=7.0$  Hz);  $^{13}\text{C}$  NMR (125 MHz,  $\text{CDCl}_3$ ):  $\delta=188.1, 158.9, 157.5, 155.2, 153.0, 144.0, 130.7, 130.5, 129.5, 125.8, 113.5, 109.6, 109.1, 97.1, 45.2, 15.3, 12.5$  ppm; IR (neat,  $\text{cm}^{-1}$ ):  $\tilde{\nu}=1744, 1610, 1561, 1499, 1422, 1266, 1123$ ; HRMS Elemental analysis calcd (%) for  $\text{C}_{19}\text{H}_{19}\text{NO}_3\text{SNa}$  [ $M+\text{Na}^+$ ]: 364.0978; found: 364.0975.

### Acknowledgements

This work was supported by the National Science Foundation (CHE-1112194). We thank Drs. Kevin Gillis and Xin Liu (UMC) for supplying separated chromaffin cells, Dr. Carol Deakynne (UMC) for helpful discussions, and Dr. Alexander Jurkevich at the Molecular Cytology Research Core Facility at University of Missouri-Columbia for assisting in confocal microscopy studies.

**Keywords:** fluorescence • molecular recognition • neurotransmitters • photoinduced electron transfer • sensors

- [1] a) G. Feng, D. Ding, B. Liu, *Nanoscale* **2012**, *4*, 6150–6165; b) Y. Yang, Q. Zhao, W. Feng, F. Li, *Chem. Rev.* **2013**, *113*, 192–270; c) J. Chan, S. C. Dodani, C. J. Chang, *Nat. Chem.* **2012**, *4*, 973–984; d) M. Chen, M. Yin, *Prog. Polym. Sci.* **2014**, *39*, 365–395.

- [2] a) D. Maurel, S. Banala, T. Laroche, K. Johnsson, *ACS Chem. Biol.* **2010**, *5*, 507–516; b) D. Srikun, A. E. Albers, C. I. Nam, A. T. Iavarone, C. J. Chang, *J. Am. Chem. Soc.* **2010**, *132*, 4455–4465; c) J. Z. Yao, C. Uttamapinant, A. Poloukhine, J. M. Baskin, J. A. Codelli, E. M. Sletten, C. R. Bertozzi, V. V. Popik, A. Y. Ting, *J. Am. Chem. Soc.* **2012**, *134*, 3720–3728.
- [3] a) T. Mineno, T. Ueno, Y. Urano, H. Kojima, T. Nagano, *Org. Lett.* **2006**, *8*, 5963–5966; b) T. Ueno, Y. Urano, K.-I. Setsukinai, H. Takakusa, H. Kojima, K. Kikuchi, K. Ohkubo, S. Fukuzumi, T. Nagano, *J. Am. Chem. Soc.* **2004**, *126*, 14079–14085; c) T. Miura, Y. Urano, K. Tanaka, T. Nagano, K. Ohkubo, S. Fukuzumi, *J. Am. Chem. Soc.* **2003**, *125*, 8666–8671.
- [4] a) P. Shieh, M. J. Hangauer, C. R. Bertozzi, *J. Am. Chem. Soc.* **2012**, *134*, 17428–17431; b) H. Sunahara, Y. Urano, H. Kojima, T. Nagano, *J. Am. Chem. Soc.* **2007**, *129*, 5597–5604; c) Y. Urano, M. Kamiya, K. Kanda, T. Ueno, K. Hirose, T. Nagano, *J. Am. Chem. Soc.* **2005**, *127*, 4888–4894.
- [5] K. E. Secor, T. E. Glass, *Org. Lett.* **2004**, *6*, 3727–3730.
- [6] K. S. Hettie, X. Liu, K. D. Gillis, T. E. Glass, *ACS Chem. Neurosci.* **2013**, *4*, 918–923.
- [7] a) E. K. Feuster, T. E. Glass, *J. Am. Chem. Soc.* **2003**, *125*, 16174–16175; b) K. Secor, J. Plante, C. Avetta, T. E. Glass, *J. Mater. Chem.* **2005**, *15*, 4073–4077.
- [8] a) S. Schenck, S. M. Wojcik, N. Brose, S. A. Takamori, *Nat. Neurosci.* **2009**, *12*, 156–162; b) N. Riveros, J. Fiedler, N. Lagos, C. Muñoz, F. Orrego, *Brain Res.* **1986**, *386*, 405–408; c) P. M. Burger, M. Ehrenfried, P. L. Cameron, P. R. Maycox, M. Baumert, F. Lottspeich, P. De Camilli, R. Jahn, *Neuron* **1989**, *3*, 715–720; d) M. Camacho, J. D. Machado, J. Alvarez, R. Borges, *J. Biol. Chem.* **2008**, *283*, 22383–22389; e) K. Zhang, Y. Chen, G. Wen, M. Mahata, F. Rao, M. M. Fung, S. Vaingankar, N. Biswas, J. R. Gayen, R. S. Friese, S. K. Mahata, B. A. Hamilton, D. T. O'Connor, *Curr. Hypertens. Rep.* **2011**, *13*, 36–45; f) J. A. Jankowski, T. J. Schroeder, E. L. Ciolkowski, R. M. Wightman, *J. Biol. Chem.* **1993**, *268*, 14694–14700; g) R. Borges, D. Pereda, B. Beltrán, M. Prunell, M. Rodríguez, J. D. Machado, *Cell. Mol. Neurobiol.* **2010**, *30*, 1359–1364.
- [9] J. Cody, S. Mandal, L. Yang, C. J. Fahrni, *J. Am. Chem. Soc.* **2008**, *130*, 13023–13032.
- [10] D. D. Méndez-Hernández, P. Tarakeshwar, D. Gust, T. A. Moore, A. L. Moore, V. Mujica, *J. Mol. Model.* **2013**, *19*, 2845–2848.
- [11] L. Wu, K. Burgess, *J. Org. Chem.* **2008**, *73*, 8711–8718.
- [12] Y. Chen, L. Wan, D. Zhang, Y. Bian, J. Jiang, *Photochem. Photobiol. Sci.* **2011**, *10*, 1030–1038.
- [13] C. Yu, L. Jiao, H. Yin, J. Zhou, W. Pang, Y. Wu, Z. Wang, G. Yang, E. Hao, *Eur. J. Org. Chem.* **2011**, 5460–5468.
- [14] E. L. Ciolkowski, B. R. Cooper, J. A. Jankowski, J. W. Jorgenson, R. M. Wightman, *J. Am. Chem. Soc.* **1992**, *114*, 2815–2821.
- [15] C. A. Parker, W. T. Rees, *Analyst* **1960**, *85*, 587–600.
- [16] M. J. Frisch, G. W. Trucks, H. B. Schlegel, G. E. Scuseria, M. A. Robb, J. R. Cheeseman, G. Scalmani, V. Barone, B. Mennucci, G. A. Petersson, H. Nakatsuji, M. Caricato, X. Li, H. P. Hratchian, A. F. Izmaylov, J. Bloino, G. Zheng, J. L. Sonnenberg, M. Hada, M. Ehara, K. Toyota, R. Fukuda, J. Hasegawa, M. Ishida, T. Nakajima, Y. Honda, O. Kitao, H. Nakai, T. Vreven, J. A. Montgomery, Jr., J. E. Peralta, F. Ogliaro, M. Bearpark, J. J. Heyd, E. Brothers, K. N. Kudin, V. N. Staroverov, R. Kobayashi, J. Normand, K. Raghavachari, A. Rendell, J. C. Burant, S. S. Iyengar, J. Tomasi, M. Cossi, N. Rega, M. J. Millam, M. Klene, J. E. Knox, J. B. Cross, V. Bakken, C. Adamo, J. Jaramillo, R. Gomperts, R. E. Stratmann, O. Yazyev, A. J. Austin, R. Cammi, C. Pomelli, J. W. Ochterski, R. L. Martin, K. Morokuma, V. G. Zakrzewski, G. Voth, P. Salvador, J. J. Dannenberg, S. Dapprich, A. D. Daniels, Ö. Farkas, J. B. Foresman, J. V. Ortiz, J. Cioslowski, D. J. Fox, *Gaussian, Inc.*, Wallingford CT, **2009**.
- [17] D. Magde, G. E. Rojas, P. G. Seybold, *Photochem. Photobiol.* **1999**, *70*, 737–744.

Received: April 16, 2014

Revised: September 10, 2014

Published online on October 24, 2014